Ore Geology Reviews 79 (2016) 241–253

Contents lists available at ScienceDirect

Ore Geology Reviews

journal homepage: www.elsevier.com/locate/oregeorev

Multi-isotope approach for the identification of metal and fluid sources of the Arroyo Rojo VMS deposit, Tierra del Fuego, Argentina

BielC.[a], SubíasI.[a,*], FanloI.[a], BillströmK.[b], AcevedoR.D.[c]

[a] Grupo Recursos Minerales, Dpto. Ciencias de la Tierra, Universidad de Zaragoza, c/ Pedro Cerbuna 12 (Edificio Geológicas), 50009 Zaragoza, Spain
[b] Department of Geological Sciences, Swedish Museum of Natural History, Frescativagen 40, Box 50007, SE-104 05 Stockholm, Sweden
[c] CADIC-CONICET, c/ Houssay 200, 9410 Ushuaia, Tierra del Fuego, Argentina

ARTICLE INFO

Article history:
Received 18 December 2015
Accepted 24 May 2016
Available online 01 June 2016

Keywords:
Arroyo Rojo
VMS
Stable isotopes
Radiogenic isotopes
Brine pool
Sub-seafloor replacement

ABSTRACT

The Arroyo Rojo deposit, located in Tierra del Fuego, is the most important polymetallic, volcanic-hosted massive sulphide in the rhyolitic belt of the Fuegian Andes. The best intercepts in drill holes indicate a true thickness of 18.6 m and concentrations of 2.2% Cu, 3.9% Pb, 14.5% Zn, 140 g/t Ag, 1.1 g/t Au). This deposit, located near the town of Ushuaia, is hosted in a Middle Jurassic volcanic and volcanoclastic sequence. Massive and semimassive bodies display stacked lenticular morphologies with disseminated mineralization in both the footwall and hanging wall. The associated hydrothermal alteration system is partially conformable with the layering of the volcanic rocks. The ores and host rocks display a penetrative tectonic foliation and were metamorphosed to greenschist facies.

Previous studies have not resulted in a consensus regarding the nature and the source of ore-forming fluids and the style of deposition of the sulphides at Arroyo Rojo. In this study, both stable and radiogenic isotopes were used develop a better understanding of these aspects of the deposit.

Hydrogen and oxygen isotopes indicate that an evolved seawater mixed with significant contributions from other fluid reservoirs such as magmatic and/or metamorphic waters was the most likely source of the ore-forming fluids. These fluids underwent significant interaction with the underlying volcanic and sedimentary rocks, which promoted partial (Sr isotopes) or full (Pb isotopes) homogenization of radiogenic isotopes. $\delta^{34}S_{CDT}$ values suggest that the sulphur was derived from several sources: biogenic reduction of seawater sulphate (BSR) in a restricted to closed basin was mixed with a heavier component derived from inorganic reduction of seawater sulphate (TRS) and possibly from sulphur leached from igneous footwall rocks and/or direct contribution from magmatic fluids.

Lateral infiltration of hydrothermal fluids resulted in the formation of a halo of semimassive to disseminated ore due to the replacement of porous, reactive glassy and breccia tuffs.

As a result of the hydrothermal circulation, two styles of mineralization are observed in the Arroyo Rojo deposit: a stringer zone and a halo of semimassive to disseminated ore corresponding to sub-seafloor replacement, and syn-sedimentary mineralization consisting of massive sulphides.

This model is consistent with the geodynamic context of the study area: a narrow, deep-marine volcano-tectonic rift parallel to the Andean side of South America and related to the initial break-up of Gondwana (ca. 145 Ma).

1. Introduction

The Arroyo Rojo polymetallic Zn-Pb-Cu-Ag volcanic-hosted massive sulphide (VMS) deposit is located at the southernmost tip of Argentina, 15 km NW of the town of Ushuaia, in the Sierra Sorondo at 54°45′S latitude and 68°06′W longitude (Fig. 1). The Arroyo Rojo deposit is the most important of several VMS prospects hosted in marine sedimentary rocks and in synsedimentary rhyolitic rocks that filled a large Mesozoic back-arc basin. A drilling programme in the Arroyo Rojo deposit in 1997 revealed ores at depths between 3 and 18.6 m (true thickness) with grades of 1% Cu, 1.4% Pb, and 3% Zn (Broili et al., 2000).

Exploration by several companies (Minera Aguilar, Polimet, Noranda, Westwin and Yamana) from 1980 to 1997 identified two main targets: Sierra Sorondo and Sierra Alvear (Fig. 1). The area as a whole is referred to as the Fin del Mundo project (Broili et al., 2000). The Sierra Sorondo and Sierra Alvear, 60 km wide by 330 km long, belong to Fuegian Andes and are separated by the Tierra Mayor Valley, a wide, U-shaped, glaciated valley (Borrello, 1972). These features are two parallel E-W-trending mountain ranges belonging to the Fuegian

* Corresponding author.
E-mail address: isubias@unizar.es (I. Subías).

http://dx.doi.org/10.1016/j.oregeorev.2016.05.019
0169-1368/

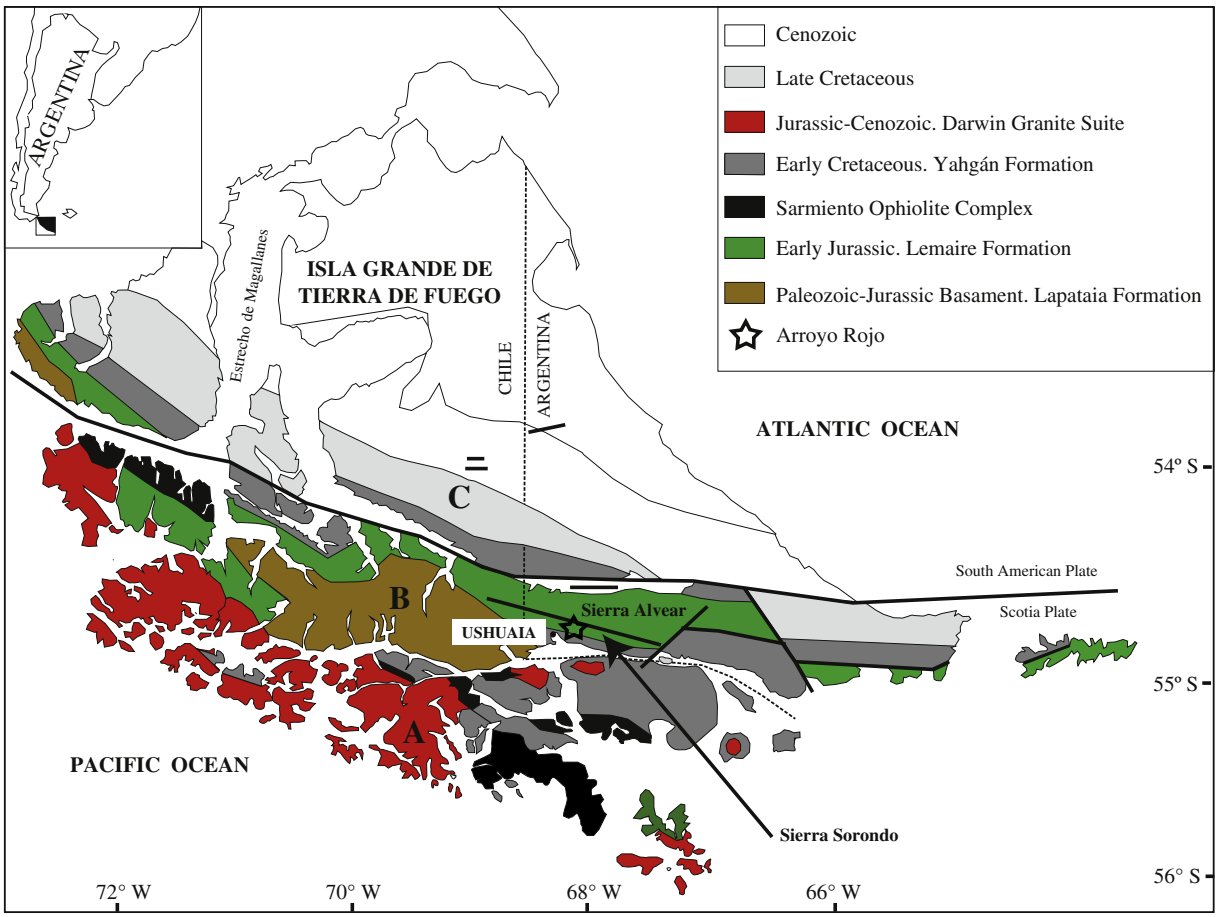

Fig. 1. Simplified geological map of the Isla Grande de Tierra de Fuego showing the location of the Arroyo Rojo deposit. Main morphostructural units: A) Fuegian Archipelago, B) Fuegian Andes and C) foothills of the Fuegian Cordillera, north of the Lago Fagnano. Sierra Alvear and Sierra Sorondo are also shown in the map.

Andes, where polymetallic sulphides are present as disseminations, stringers, and semimassive to massive lenses that are exposed across extensive areas.

Most of the previous work on the VMS mineralization in the Fin del Mundo project addressed the general characteristics of these sulphides and their general geology (Ametrano et al., 2000; Broili et al., 2000; Acevedo et al., 2005). Biel et al. (2010, 2012) reported field observations and the textural relations, mineral chemistry, and alteration architecture of the Arroyo Rojo VMS deposit with the goal of identifying the deposit style and developing exploration criteria.

According to Ametrano et al. (2000) and Broili et al. (2000), the Arroyo Rojo deposit exhibits many of the geologic features of mound style VMS deposits (Large, 1992). During the previous five years, detailed geological, mineralogical, and geochemical studies of the Arroyo Rojo deposit lead Biel et al. (2010) and Biel (2011) to suggest that the ore formed in a brine pool according to the criteria of Solomon et al. (2004). Thus, there is yet no widespread agreement regarding the nature and source of the Arroyo Rojo ore fluids.

The present study focused mainly on the origin and source of mineralizing components and the conditions of ore deposition. Stable (H, O, S) and radiogenic (Pb, Sr) isotopes were used to better understand these aspects of the Arroyo Rojo deposit.

2. Geological setting

2.1. Regional geology

The study area is located on the Isla Grande de Tierra del Fuego (Fig. 1), which is the largest of the Fuegian Archipelago islands and is located in southern Argentina between latitudes 53 and 56°S and longitudes 66 and 72°W. The Isla Grande is situated on the Scotia Plate near the boundary with the South American Plate. The geology of this area is related to a succession of extensional to compressive and transcurrent tectonic regimes related to three major orogenic cycles: the Gondwanian (Palaeozoic to Triassic), Patagonian (Jurassic to Early Cretaceous), and Andean (Upper Cretaceous to Cenozoic) cycles.

The Isla Grande de Tierra del Fuego belongs to the Fuegian Andes, a mountain system that is bounded by E-W and NW-SE faults. This geological province comprises three morphostructural units (Fig. 1): (A) the Fuegian Archipelago, formed by several intrusions during the Cretaceous and the Cenozoic, (B) the Fuegian Cordillera, and (C) the foothills of the Fuegian Cordillera, north of the Lago Fagnano (e.g., Caminos, 1980; Olivero and Martinioni, 2001).

The VMS deposits of the Fin del Mundo district are located in the Fuegian Cordillera, where three formations have been recognized:

The basement rocks, which are assigned to the Lapataia Formation (Fig. 1), form the core of the Fuegian Cordillera and are exposed in the Darwin Cordillera (Chile) and Bahía Lapataia (Argentina). They consist of strongly folded fine-grained phyllites intercalated with amphibolite and quartz-sericite to biotite-garnet schists. Regional peak metamorphism is defined by staurolite, kyanite, and sillimanite (Dalziel and Brown, 1989). The age of the Lapataia Formation, based on isotopic and fossil data, is regarded as late Palaeozoic to Middle Jurassic (Hervè et al., 1981).

The Lapataia Formation is unconformably overlain by (i) a submarine volcanic-sedimentary succession (the Lemaire Formation, known as Tobífera Formation in Chile) and (ii) a volcaniclastic apron of deep-marine andesite-rich turbidites and mudstones (the Yahgán Formation).

The Lemaire Formation (Kranck, 1932) forms a submarine volcanic-sedimentary complex and is composed of silicic pyroclastic rocks (rhyolitic ignimbrites and tuffs) with interbedded epiclastic rocks (conglomerates, turbidites, chert, black shales and calcareous layers with minor mafic and intermediate lavas (Hanson and Wilson, 1991; Pankhurst et al., 1998). Also, Fildani and Hessler (2005) and Calderón et al. (2007) identified pillow basalts of the Sarmiento Ophiolite Complex (Fig. 1) interbedded with Lemaire Formation tuffs. The Lemaire Formation is strongly deformed, and a penetrative cleavage has completely obliterated the original stratification in the fine-grained facies.

Samples from the Sarmiento Ophiolite Complex yielded an age of ~150 Ma, whereas two samples of silicic pyroclastic rocks from the Lemaire Formation yielded ages of 148 and 142 Ma, indicating contemporaneous bimodal volcanism (Calderón et al., 2007; U—Pb ages of zircons).

Recent work (Hervé et al., 2007) suggests that the development of a juvenile arc batholith, the Darwin Granite Suite, was coeval with the voluminous rhyolitic ignimbrites of the Lemaire Formation as well as with the quasi-oceanic mafic floor, which constitutes the Sarmiento Ophiolite Complex. Hervè et al. (1981) reported a Rb—Sr age of 157 ± 8 Ma for whole rock samples from the Darwin Granite Suite, which is similar to U—Pb ages obtained from zircons (164.1 Ma; Mukasa and Dalziel, 1996).

The Yahgán Formation (Kranck, 1932) consists of coarse breccias and conglomerates, sandstones, sandy and silty turbidites, black tuffaceous mudstones and tuffs intruded by basaltic rocks of tholeiitic-calc-alkaline affinities. The contact with the Lemaire Formation is predominantly tectonic and locally, unconformable. Fossils in the Yahgán Formation suggest a Tithonian-Neocomian (~144 Ma) age of this basal portion and a late Albian (~100 Ma) age of this upper portion (Olivero and Malumián, 2008, and references therein). Granitic-dioritic rocks younger than the main deformation have been dated to between 70 and 90 Ma (zircon U-Pb and muscovite $^{40}Ar/^{39}Ar$ ages; Mukasa and Dalziel, 1996).

This succession reveals contrasting Mesozoic-Cenozoic tectonic regimes: Jurassic rifting responsible for the deposition of the Lemaire Formation, evolved into a back-arc basin coeval with mafic volcanism and marine sedimentation of the Yahgán Formation. The Late Cretaceous deformation (isoclinal folding) and metamorphism of these rocks indicate a compressional tectonic regime that resulted in the closure of the marginal basin. The metamorphic grade reaches the lower greenschist facies (Biel et al., 2007; Biel, 2011), and a widespread prehnitization specifically affected the Yahgán Formation (Caminos et al., 1981).

2.2. Geology of the deposit

Mapping, re-evaluation of drilling data and sampling of the Arroyo Rojo deposit allowed Broili et al. (2000), Biel et al. (2010) and Biel (2011) to delineate a 200-m-long zone of discontinuous mineralized bodies. There are two concordant massive lenses exposed along strike: a 70-m-long western lens and a 35-m-long eastern lens, separated by a concealed, slightly sulphidic body (Fig. 2A). The fragmentation of the massive sulphide lenses was due to deformation. Drilling confirmed the presence of two additional massive sulphide lenses at depth and that the lenses are more continuous at depth than at the surface.

The ores and their host rocks experienced greenschist metamorphism as suggested by their mineral associations (Caminos, 1980; Olivero and Martinioni, 2001) and the crystallinity index of their micas and chlorites (Biel et al., 2007). The Arroyo Rojo deposit is located in the core of an anticlinal structure and constitutes the footwall of the major stacks of the regional thrust systems. Penetrative structural fabrics are located in a local shear zone associated with the main faults marked by the presence of mylonitic foliation.

The ore bodies exhibit a stratiform morphology, consisting of stacked lenses and disseminated mineralization in both their footwall and hanging wall. Stringer mineralization is also present. The internal structure of the ore lenses is characterized by the occurrence of massive, semi-massive and banded sulphide facies, consisting of fine-grained pyrite and sphalerite-rich laminae. In the upper part of the ore bodies, there is an overall decrease in sphalerite and an increase in chalcopyrite, which forms forming a compositional layering with pyrite that is disrupted by boudinaged sphalerite porphyroblasts. In most places, the layers are parallel to the regional foliation as a result of deformation, although there are primary sedimentary features preserved in places. Locally, deformation promoted mylonitization and even recrystallization, generating elongated pyrite crystals following the regional foliation.

The host rock corresponds to volcanic portion of the Lemaire Formation. Despite its deformation and metamorphism, protoliths are recognizable in the Arroyo Rojo deposit (Fig. 2A). The volcanic and volcaniclastic sequence, in upward succession, consist of a lower rhyolite, dacite, ignimbrite, tuff, and an upper rhyolite (Fig. 2B): (1) The lower rhyolite (Fig. 3A) is characterized by millimetric elongate quartz and K-feldspar crystals that comprise <5% of the rock. This rock does not exhibit flow banding and is interpreted as a dome deposit. (2) The *dacite* exhibits elongate crystals. Under the microscope, this rock is composed of Na plagioclase phenocrysts exhibiting twinning, growth zonation and sericite alteration, and some quartz phenocrysts (Fig. 3B). The dacite unit has been observed only in drill cores (Fig. 2C). (3) Fiammes are the main macroscopic characteristic of the *ignimbrite* (Fig. 3C). Under the microscope, this rock exhibits a well-developed eutaxitic texture of flattened and welded pumice lapilli in a pale-brown ash matrix. The groundmass is partially replaced by chlorite, clinozoisite and sericite. (4) The *tuff units* host the massive sulphide mineralization. They include a wide range of volcaniclastic rocks that have been subdivided on the basis of the crystal/glass/clast proportions into crystal, vesicular (Fig. 3D), glassy and brecciated tuffs (Fig. 3E). (5) Unlike the lower rhyolite, the upper rhyolite (Fig. 3F) exhibits flow banding and is devoid of phenocrysts. Under the microscope, it contains up to 1% of modal quartz and feldspar phenocrysts, and 5% of vesicles generally filled with quartz and locally, with calcite. Its glass matrix, which exhibits flow banding, is partially to completely replaced by fine-grained quartz and sericite. The upper rhyolite has only been observed in drill cores. All the above units are unconformably overlain by (6) the *hyaloclastic andesite* that belong to Yahgán Formation.

Deformation has led to the development of mylonite (Fig. 3G) and also rhyolitic rocks may show strong signs of metamorphism (Fig. 3H).

The regional seafloor alteration, characterized by clinozoisite, Fe-chlorite, titanite, quartz and albite (Biel et al., 2012), is partially obliterated by hydrothermal alteration (Biel et al., op. cit.). This hydrothermal alteration is semi-conformable and includes: (1) a widespread *silicification* (Fig. 3I) throughout the volcanic sequence. Its intensity is highly variable and tends to decrease within the massive sulphides zones; (2) *chloritization* (Fig. 3J) that is the most pervasive alteration and as a result, chloritite (an altered rock composed of more than 90% modal chlorite (Schermerhorn, 1978) is commonly located beneath massive sulphides bodies; (3) *sericitization* is less pervasive in the footwall and more extensive in the hanging wall; (4) *local albitization* characterized fine-grained replacements of volcanic glass and phenocrysts of the rhyolitic rocks, as well as filling veins (Fig. 3K) and as rims and patches replacing primary K-feldspar in weakly altered volcanic rocks; and (4) *rare carbonization* (Fig. 3L) that occurs as spar crystals within sulphides, as filling veinlets and pumice vesicles in the mineralized horizons.

Mg-chlorite and phengitic white mica are typically present in the vicinity of the Arroyo Rojo ore lenses. Biel et al. (op. cit.) classified the chlorite-bearing hydrothermal alteration in the Arroyo Rojo prospect into regional, distal, and proximal (related to semimassive and massive ores) zones based on the proximity to the ore and the Fe/Fe + Mg ratio (F/FM). Chlorite near the sulphide lenses is richer in Mg (F/FM = 0.11 ± 0.06) than that in the distal (F/FM = 0.39 ± 0.10) and regional (F/FM > 0.52) alteration assemblages.

The mineral assemblages (Fig. 4) of the ore lenses exhibit a high (Zn + Pb)/Cu ratio and consist primarily of pyrite and sphalerite, with

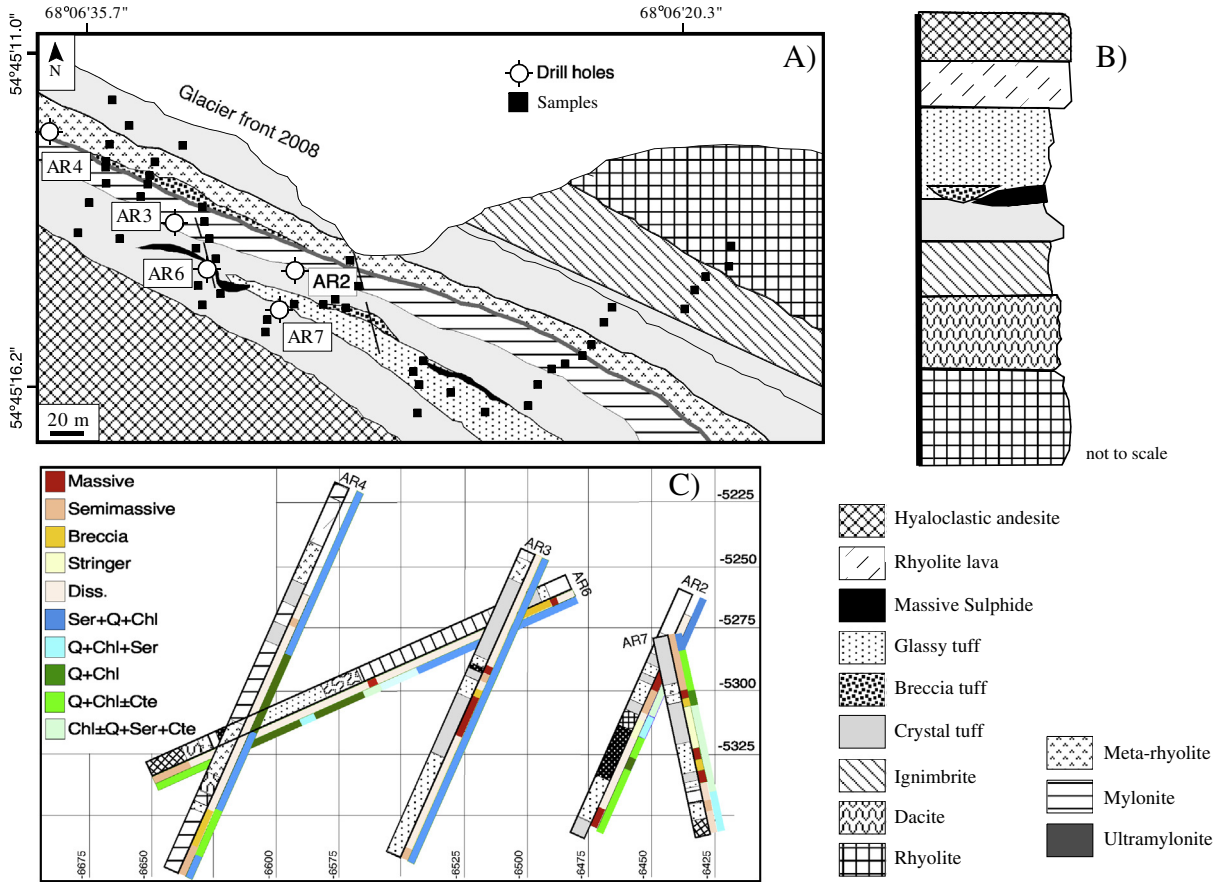

Fig. 2. A) Geological map of the Arroyo Rojo deposit showing the location of drill holes and surface samples. Massive sulphide lenses are drawn in red; B) Local stratigraphy of the Lemaire Formation at the Arroyo Rojo deposit.; C) Drill core sketch map showing the relation between mineralization, alteration, and lithotypes (Q: Quartz; Chl: Chlorite; Ser: Sericite; Cte: Calcite; Diss.: Disseminated ores).

lesser amounts of galena and chalcopyrite, and rare pyrrhotite, arsenopyrite, tetrahedrite and bournonite. Pyrite is the dominant iron sulphide, and the pyrrhotite content decreases upward markedly. The absence of sulphates and zone refining is noteworthy. Zone refining develops due to a large thermal gradient, from hot at the base to cooler at the top (Eldridge et al., 1983), which causes mineralizing fluids entering the base of the lens to progressively deposit Cu within the base and interior of the lens and to re-dissolve Zn and Pb, (+/−Au, Ag), transport them upward, and concentration them at the top.

To evaluate the wide textural range of the sulphide ores, we have established the following three textural groups: *sedimentary-diagenetic textures* such as framboids, polyframboids and banding in pyrite (Fig. 4A), *hydrothermal textures* such as growth twins preserved in coarser sphalerite and chalcopyrite grains (Fig. 4B), and deformation and metamorphic textures such as brittle failure in pyrite (Fig. 4C) and well-developed polygonal recrystallization to finer grains with triple junctions in sphalerite (Fig. 4D).

Fluid inclusions in quartz from Arroyo Rojo deposit are aligned primarily along fractures and are clearly secondary (Fig. 4E). Primary fluid inclusions are scarce and small (<3 μm), typically present as scattered and isolated inclusions in quartz and have regular forms, such as negative crystal and polygonal shapes. The morphology and optical properties of the solids in the inclusions indicate that halite is the daughter mineral (Fig. 4F).

3. Temperature of mineralization

We have applied the empirical geothermometer of Cathelineau (1988) to estimate the formation temperatures of the chlorite in the different alteration assemblages recognized in this study (Table 1). Chlorite from the mineralized and proximal zones yielded temperatures (254° and 260 °C, respectively) lower than chlorite from the distal (averaging T is 285 °C) and regional assemblages (350 °C).

The Fe/Zn ratio in sphalerite can be used as a geothermometer (Keith et al., 2014) in inactive vent sites and weakly metamorphosed fossil VMS deposits. After excluding the samples affected by chalcopyrite disease and pyrite inclusions, Biel (2011) reported Fe contents in sphalerite between 1.6 and 6.0 wt.% ($n = 93$). Sphalerite precipitation temperatures were found to fall between 247 °C and 307 °C, with no recognized systematic variation of the Fe content in sphalerite with depth, style of mineralization (massive, semimassive, disseminated) or textures (primary, deformation or recrystallization).

4. Sampling and analytical methods

Analysis was performed on samples collected from outcrops and drill cores (Fig. 2) with regard to differently dominant minerals, ore styles (massive, semimassive, disseminated) and textural types (deformation, metamorphism, diagenetic, primary) following Biel et al. (2010). Samples of weakly altered or unaltered host rocks of the Lemaire Formation were collected for comparisons with non-mineralized areas. The latter samples are referred to in this paper as regional samples.

Rb, Sr, U, Th and Pb concentrations were determined at Activation Laboratories (Ancaster, Ontario, Canada) via ICP and NAA (see INAA, total digestion - ICP, lithium metaborate/tetraborate fusion – ICP at www.actlabs.com for details of the methods).

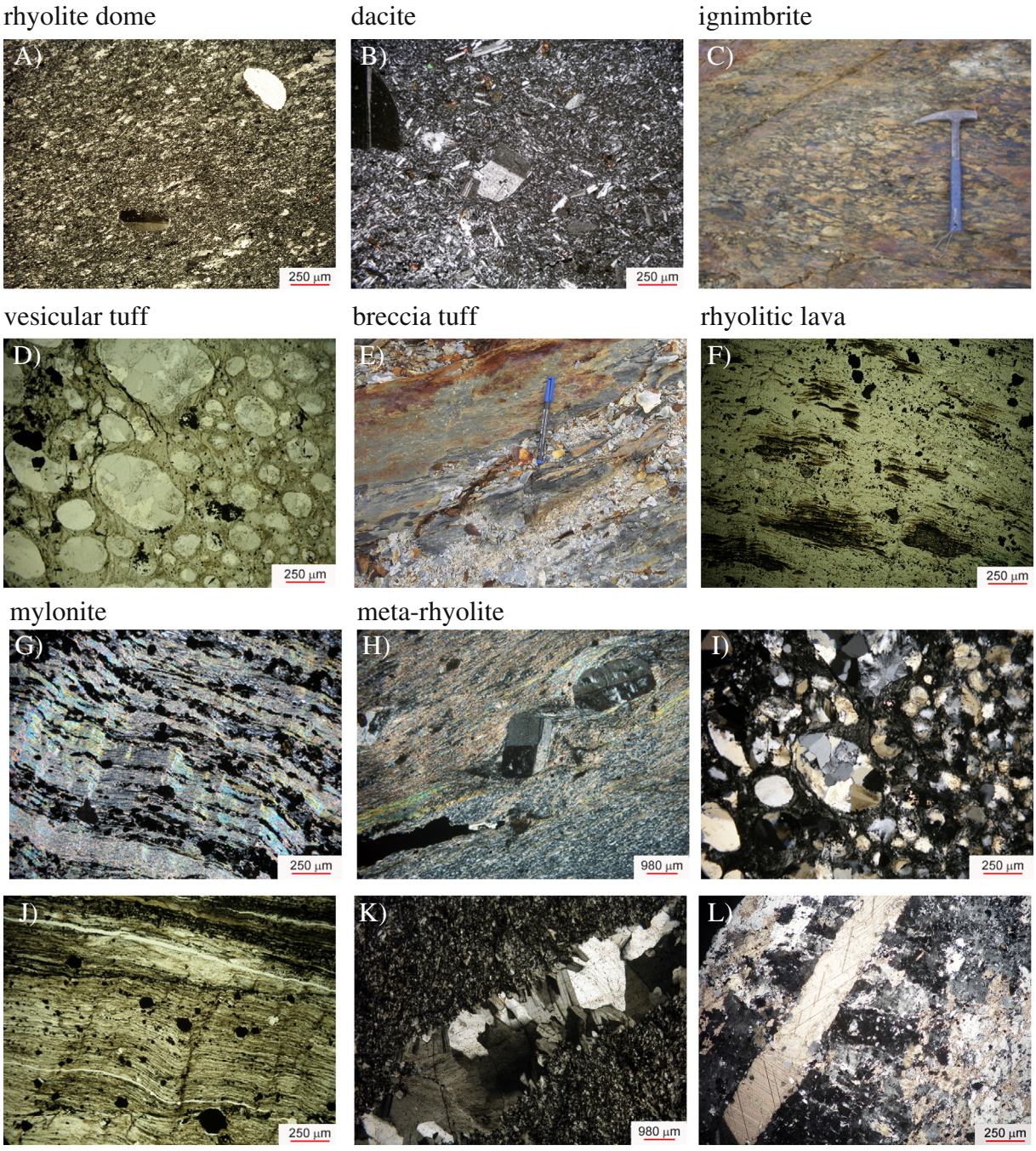

Fig. 3. A) Rhyolite; B) Diorite: Na-feldspar phenocrysts and microphenocrysts in a matrix of feldspar locally replaced by quartz-sericite; C) Field view of ignimbrite with flattened and welded pumice lapilli in a dark matrix with fiammes totally replaced by chlorite; D) Pumice shard with millimetric devitrified, glass vesicles and totally replaced by chlorite; E) Field view of tuffaceous breccia with millimetric to centimetric altered tuff clasts in a darker quartz-pyritic matrix; F) Rhyolitic lava with fluidal texture; G) Preferred oriented mica and quartz in two main deformational stages in mylonite; H) Metarhyolite consisting of feldspar phenocrysts in an oriented quartz-micaceous matrix; I) devitrified glass vesicles totally replaced by mono- and polycrystalline quartz under crossed polars; J) chloritite with pyrite disseminations under parallel polars; K) open space adularia filling in an albitized rock under crossed polars; L) quartz and calcite association in a mineralized rock also showing sparry calcite as fracture fillings under crossed polars.

Stable isotope ratios were determined at the Laboratorio de Isótopos Estables of the Universidad de Salamanca (Spain). Thirty-nine $\delta^{34}S$ determinations on all textural types of ore sulphides were performed via Nd-YAG laser ablation (see Fallick et al., 1992 for details on the method). Sulphur as Ag_2S was recovered from underlying host rocks by reaction with HCl + $CrCl_2$, using a modified version of the method of Canfield et al. (1986) and Hall et al. (1988). The results are reported in the delta ($\delta^{34}S$) permil notation relative to Canyon Diablo Troilite (CDT). Replicate analyses of reference standards yielded an average reproducibility of ±0.3‰.

Hydrogen and oxygen isotope analyses were performed on fifteen chlorite samples. Concentrates were obtained using a diamond coated dental drill, were selected to represent all chlorite types identified by Biel et al. (2012), and were purified by handpicking under the binocular microscope. Hydrogen was extracted by induction heating (1200 °C) under vacuum in a previously degassed platinum crucible containing the sample. Water produced during dehydroxylation was converted to H_2 over U metal at 800 °C in a multiple-pass system and the yield was measured using a manometer connected to a Toepler pump for transport of the H_2. Oxygen isotope compositions were determined using

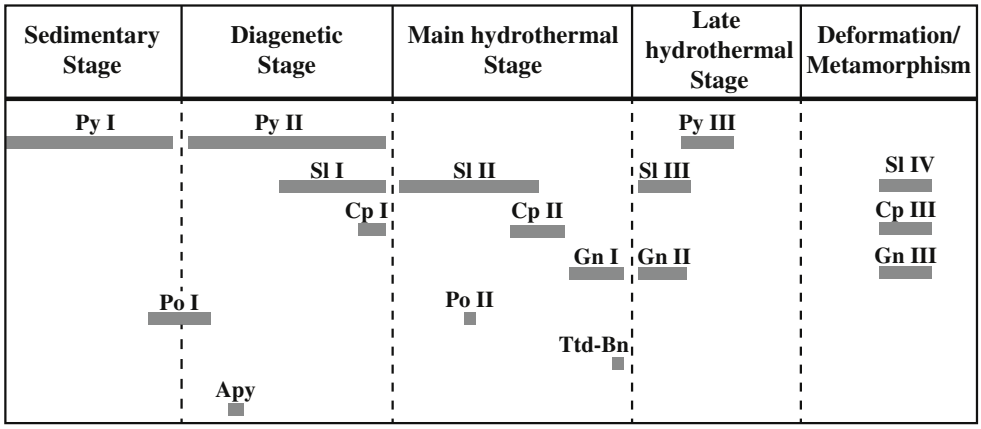

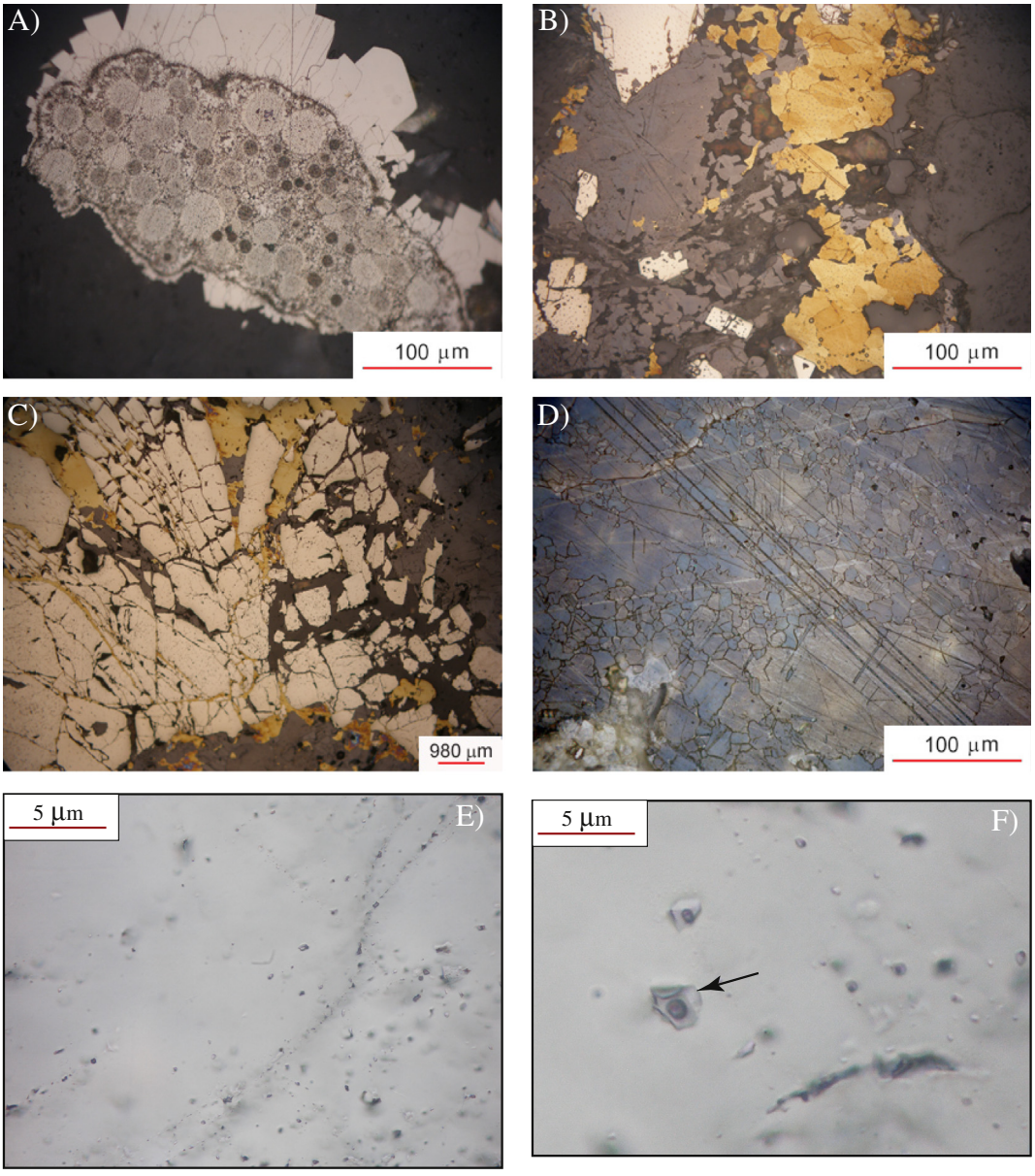

Fig. 4. Paragenetic scheme and polarized reflected-light microphotographs of some ore samples used in this study showing primary and secondary textures. A) Sedimentary and diagenetic stage: euhedral pyritic radial overgrowths over polyframboidal cores. Specimen etched with HNO_3; B) Late hydrothermal stage: growing twinning in chalcopyrite and sphalerite along with a pyrite crystal. Specimen etched with diluted HNO_3; C) Oriented fractures in pyrite with incipient developing of cataclastic flow; D) Annealing twins developed in triple junctions of recrystallized sphalerite grains. Specimen etched with diluted HNO_3.

Table 1
$\delta^{18}O$ and δD signatures of chlorites associated with the Arroyo Rojo deposit and estimated $\delta^{18}O$ and δD values for an ore fluid in isotopic equilibrium with chlorite. Chlorite geothermometry was calculated by means of Cathelineau's (1988) equation using the obtained Mg/Fe ratios.

Sample	Min.	$\delta^{34}S_{CDT}$ (‰)	Ore petrography	Ore style
AR2-12-42.8C1	Py	−0.8	Cataclastic (D)	Semimassive
AR2-12-42.8C51	Py	0.2	Cataclastic (D)	Semimassive
AR2-12-42.8C51	Sp	−0.9	Deformation twins and recrystallization (D)	Semimassive
AR2-70.6C4	Gn	−6.0	Grain-boundary sliding (D)	Semimassive
AR3-88.4C12	Cpy	−1.5	Deformation twins (D)	Massive
AR3-88.4C3	Py	−2.7	Cataclastic (D)	Massive
AR7-45-160.7C4	Py	1.0	Grain-boundary sliding (D)	Semimassive
AR7-45-160.7C4	Py	1.3	Grain-boundary sliding (D)	Semimassive
AR2-39-142.6C1	Py	2.6	Recrystallization and annealing twins (M)	Massive
AR3-88.4C32	Sp	−1.1	Annealing twins (M)	Massive
AR3-49-180.5C2	Sp	−2.0	Annealing twins (M)	Disseminated
AR3-49-180.5C5B	Sp	−2.9	Annealing twins (M)	Disseminated
AR6-105-364.9C1	Po	−27.6	Polygonal textures (M)	Semimassive
AR6-105-364.9C2	Po	−27.6	Polygonal textures (M)	Semimassive
AR6-105-364.9C3	Po	−27.5	Polygonal textures (M)	Semimassive
AR7-14-48.1C4	Sp	2.3	Annealing twins (M)	Massive
AR2-39-142.6C2	Py	−0.7	Recrystallized euhedral grains (*D*-H)	Massive
AR4-100.4C1	Py	−13.7	Elongated recrystallized grains (D-H)	Disseminated
AR4-100.4C2	Py	−15.0	Elongated recrystallized grains (D-H)	Disseminated
AR4-100.4C3	Py	−15.1	Elongated recrystallized grains (D-H)	Disseminated
AR6-170C2	Py	−12.1	Recrystallized euhedral grains (D-H)	Massive
AR6-170C7	Py	−12.0	Recrystallized euhedral grains (D-H)	Massive
AR2-12-42.8C53	Sp	0.0	Growth twins (P)	Semimassive
AR2-12-42.8C43	Cpy	−0.9	Growth twins (P)	Semimassive
AR2-70.6C2	Py	−3.6	Framboidal (P)	Semimassive
AR3-1-5C1A	Py	−8.6	Framboidal (P)	Disseminated
AR3-1-5C1B	Py	−8.3	Framboidal (P)	Disseminated
AR3-1-5C2	Py	−7.8	Framboidal (P)	Disseminated
AR3-88.4C64	Sp	0.5	Growth twins (P)	Massive
AR3-88.4C64	Cpy	−0.4	Growth twins (P)	Massive
AR4-198.5C2	Py	−21.6	Recrystallized framboids to euhedral (P)	Disseminated
AR4-238C1	Py	−7.1	Colloform (P)	Semimassive
AR4-238C3	Py	−16.3	Colloform (P)	Semimassive
AR4-238C4	Py	−12.8	Colloform (P)	Semimassive
AR7-45-160.7C4	Cpy	−1.0	Growth twins (P)	Semimassive
LM-5	WR	−0.6		Siltstone
LM-4	WR	−1.8		Siltstone
LM-1	WR	−9.6		Siltstone

[1] 250 °C for deformed sulphides,
[2] 335 °C for annealed sulphides and
[3] 144 °C and
[4] 135 °C for primary sulphides.

the fluorination laser technique (Sharp, 1990). The oxygen and hydrogen isotopic values are reported as permil deviations relative to standard mean ocean water (V-SMOW). The analytical precision of the isotopic analyses was estimated at ±1‰ for δD and better than ±0.2‰ for $\delta^{18}O$.

Radiogenic isotope analyses were conducted at the Department of Geological Sciences at the Swedish Museum of Natural History (Stockholm, Sweden). Lead isotope compositions were determined for 13 ore sulphide samples representing all depositional stages, for 3 chlorite samples and for 12 volcanic and detrital whole-rock samples. Strontium isotopic compositions of 12 whole-rock and 9 chlorite samples were also performed. Chemical separation of lead from the sulphides involved dissolution-evaporation in HNO_3 at 100 °C, whereas the whole-rock and chlorite samples were taken up in a HF/HNO_3 mixture following the Teflon bomb method of Krogh (1973) at 205 °C. Purified Pb and Sr were obtained using ion-exchange columns and anodic electrodeposition. Pb isotopic ratios were determined using a Micromass ISOPROBE mass spectrometer, and the reproducibility of these data was approximately ±0.1% (2σ). The Sr isotopic ratios were measured using a Triton multi-collector (TIMS) mass spectrometer. The precision and reproducibility were confirmed using the SRM981, SRM987, BCR-1 and La Jolla standards.

5. Results

5.1. S, O and H isotopes

The sulphur isotope findings from the Arroyo Rojo deposit are listed in Table 2 and plotted in Fig. 5. The S isotopic values are relatively homogeneous regardless of their style of mineralization; the disseminated ores in the footwall and hanging-wall have lighter $\delta^{34}S_{CDT}$ values (−21.6 to −2.0 ‰), whereas these values are heavier in the massive ores (−12.1‰ to +2.6‰). One pyrrhotite sample from a semimassive body (AR6–105-364.9) yielded remarkably light values (−27.6‰; mean value of spots in three separate grains). Leaving out this extreme value, a tendency is suggested for a shift (Fig. 5B) towards heavier isotopic values is observed with the transition from sedimentary and hydrothermal-diagenetic textures (−21.7 to +0.5‰) to samples with signs of metamorphism (−2.9 to +2.6‰). All samples with $\delta^{34}S_{CDT}$ values below −10‰ came from drill holes AR4 and AR6, which correspond to the deeper mineralized lens.

Three siltstone samples from the Lemaire Formation yielded $\delta^{34}S_{CDT}$ values between −9.6 and −0.6‰. These samples were collected in non-mineralized areas, and a petrographic examination did not reveal any disseminations of sulphides.

Sulphur isotope equilibrium temperatures were calculated from pyrite-sphalerite and chalcopyrite-sphalerite pairs using the equations of Kajiwara and Krouse (1971). Despite the scarcity of data, the mineral pairs exhibiting primary textures yielded lower temperatures (~140 °C) than the samples exhibiting annealed and metamorphic textures (between ~250° and 335 °C).

The $\delta^{18}O_{chlorite}$ values range between +5.1 and +13.9 ‰ (Table 1). The hydrothermal chlorite samples from the zones of massive and semimassive mineralization yielded $\delta^{18}O_{V\text{-}SMOW}$ values between +5.1 and +11.7‰, the proximal zones yielded $\delta^{18}O_{chlorite}$ values between +7.4 and +13.1 ‰, and the distal and regional zones yielded values between +9.1 and +13.9‰. The oxygen data indicate a weak trend of isotopically lighter chlorites in the massive and semimassive settings than

Table 2
Sulphur isotope data for ore minerals from the Arroyo Rojo deposit. Sulphide pairs used for isotope geothermometry are marked in italics and calculated temperatures are shown at the footnote. Abbreviations: D = deformation; M = metamorphism; diag = diagenetic; P = primary; Py: pyrite; Sp: sphalerite; Gn: galena; Cpy. Chalcopyrite; Po: pyrrhotite; WR: whole rock. C1, C2, C3, etc. correspond to different grains in the same polished section. The letters (A, B) refer to different spots within a single grain.

Sample	Ore Proximity	$\delta^{18}O_{SMOW}$ (‰)	δD_{SMOW} (‰)	$\delta^{18}O$ fluid (‰)	δD fluid (‰)	Mean T
AR6-202C1	Regional	13.9	−82.6	15.1	−49.1	350 °C
AR6-262C1	Regional	10.2	−86.8	11.4	−53.3	
AR6-308	Distal	13.4	−85.6	12.8	−49.7	285 °C
AR2-57C1	Distal	9.6	−66.0	9.0	−30.1	
AR2-57C4	Distal	9.1	−68.9	8.5	−33.0	
AR2–105C2	Proximal	7.4	−62.9	4.2	−25.9	260 °C
AR2-75C1	Proximal	9.1	−68.7	5.9	−31.7	
AR2-75C2	Proximal	11.0	−67.0	7.8	−30.0	
AR6-139C1	Proximal	11.3	−89.7	8.1	−52.7	
AR6-139C3	Proximal	13.1	−70.9	9.9	−33.9	
AR7-133C2	Proximal	8.3	−54.0	5.1	−17.0	
AR7-134C3	Semimassive	5.1	−53.5	1.6	−16.2	254 °C
AR7-134C2	Semimassive	5.1	−53.9	1.6	−16.6	
AR3-3C1	Massive	11.7	−42.4	8.2	−5.1	
AR7-94.8	Massive	7.7	−59.9	4.2	−22.6	

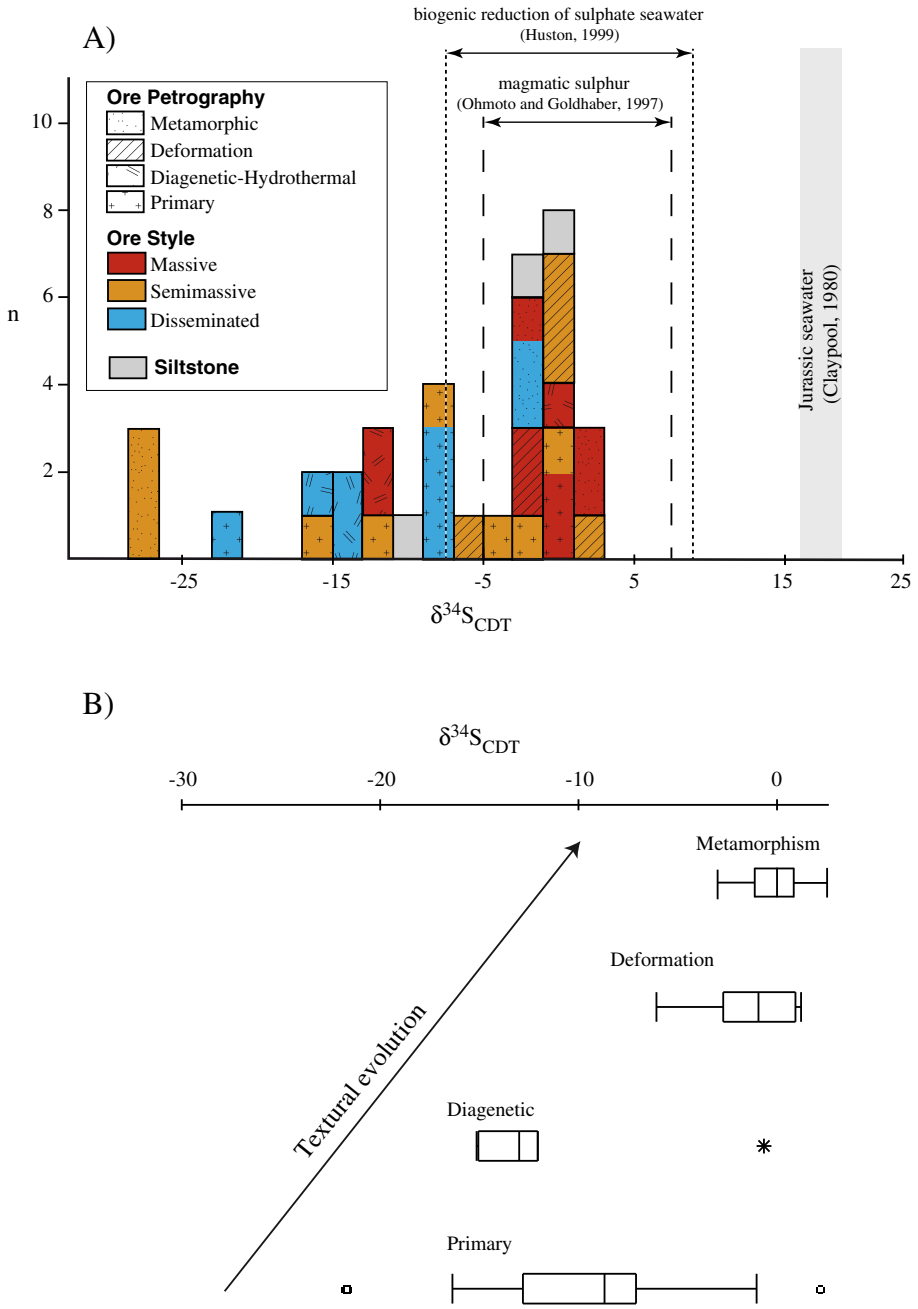

Fig. 5. A) Frequency histogram showing the range of the $\delta^{34}S$ values for the analysed sulphides by ore petrography and ore style and plausible reservoirs. B) Boxplot diagram of the $\delta^{34}S$ values after textural type. Boxplots define the median (horizontal line across the box), percentiles, whiskers, and outliers; shaded area on each box indicates 95% confidence interval bounds around its median.

in the other chlorites, whereas the hydrogen data display a clearer correlation with proximity to the ore. The δD isotopic values are heavier in the zones of massive and semimassive mineralization (−42.4 to −59.9‰), than in the proximal (−54.0 to −89.7‰), distal (−66.0 to −85.6‰) and regional alteration chlorite samples (−82.6 to −86.8‰).

The isotopic composition of water in isotopic equilibrium with the chlorite was calculated based on temperatures estimated using the geothermometer of Cathelineau (1988) and on the fractionation equations of Graham et al. (1987) and the chlorite-water fractionation equations of Savin and Lee (1988) for Mg-rich, Mg-intermediate and Mg-poor compositions. The fluids in equilibrium with the chlorites in the zones of semimassive and massive mineralization (Table 1) yielded $\delta^{18}O$ values between +1.6 and +8.2‰. The compositions of fluids in equilibrium with the proximal chlorites range between +5.1 and +9.9‰, and those of the distal and regional chlorites range between +8.5 and +15.1‰. The δD values of water in equilibrium with the chlorite in the ore zone range between −5 and −23‰, whereas these values are lighter in the proximal zones (−17 to −53‰) and distal and regional zones (−30 to −53 ‰).

5.2. Pb isotopes

The lead isotope data from the sulphides, which included one galena sample, and chlorite (Table 3) are homogeneous and typically within the range of analytical uncertainty. Galena is a true common lead phase (i.e., the U/Pb and Th/Pb ratios are literally zero, which means that the lead isotopic composition does not change over time), whereas the other sulphides may contain non-negligible amounts of U and Th. To

Table 3
Displayed isotope ratios reflect the lead component present in the ore (based on measured sulphide and chlorite data) and in the sedimentary and volcanic roks from Lemaire Formation. Asterisks indicate those samples with measured U, Th and Pb concentration data. Negative SK and CR values are not shown (SK: Stacey and Kramers, 1975; CR: Cumming and Richards, 1975).

Sample	Type	$^{206}Pb/^{204}Pb$	$^{207}Pb/^{204}Pb$	$^{208}Pb/^{204}Pb$	μ	ω	SK	CR
AR2-20-70.6	Gn	18.641	15.639	38.478	9.83	36.88	69	119
AR2-42.8C4	Cp	18.648	15.646	38.500	9.84	36.99	79	115
AR2-42.8C5-1*	Sph	18.630	15.628	38.443	9.82	36.70	54	125
AR2-42.8C5-2	Sph	18.648	15.643	38.495	9.84	36.96	73	115
AR2-42.8-1	Py	18.634	15.640	38.484	9.82	36.91	77	123
AR2-42.8-2	Py	18.630	15.641	38.495	9.82	36.96	82	125
AR3-180.5*	Sph	18.637	15.641	38.484	9.83	36.91	77	121
AR3-88.4C1	Cp	18.639	15.638	38.495	9.83	36.96	55	120
AR3-88.4C3	Py	18.643	15.643	38.496	9.84	36.97	53	118
AR3-88.4C3	Sph	18.643	15.643	38.496	9.84	36.97	76	118
AR3-88.4C6	Cp	18.642	15.644	38.495	7.21	36.96	53	118
AR3-88.4C6	Sph	18.640	15.642	38.490	9.83	36.94	76	119
AR4-238.	Py (euhedral)	18.692	15.693	38.647	9.90	37.74	145	90
AR4-238*	Py	18.648	15.646	38.479	9.84	36.88	79	115
AR6-171	Py	18.629	15.647	38.518	9.82	37.08	92	130
AR6-364.9*	Po	18.659	15.654	38.497	9.89	37.11	119	95
AR2-1-3C3	Chl (mass)	18.729	15.650	38.568	9.95	37.34		68
AR7-38C1	Chl (sm)	18.644	15.642	38.483	9.84	36.90	52	117
AR2-105C2	Chl (prox)	18.652	15.638	38.497	9.85	36.97	47	112
AR6-139C3	Chl (prox)	18.727	15.642	38.542	9.95	37.20		70
AR6-139C2	Chl (prox)	18.729	15.646	38.555	9.95	37.27		68
AR7-133C1	Chl (prox)	18.633	15.632	38.452	9.82	36.75	59	123
AR2-57C3	Chl (distal)	18.629	15.635	38.466	9.82	36.82	61	126
AR2-57C2	Chl (distal)	18.642	15.642	38.487	9.84	36.92	53	118
AR6-202C3	Chl (regional)	18.852	15.642	38.600	10.11	37.50		
AR6-262.5C3	Chl (regional)	18.960	15.642	38.727	10.25	38.14		
LMO*	Rhyolite	18.140	15.610	38.220	9.18	40.47		
BC6-4*	Rhyolite	18.680	15.640	38.490	9.89	38.58		
BS1-4*	Rhyolite	19.110	15.710	38.610	10.45	40.13		
PC4	Xtal tuff	18.680	15.640	38.530	9.89	38.60		
BS1-6*	Xtal tuff	18.720	15.660	38.490	9.94	38.57		
LM-1	Sandstone	18.350	15.630	38.240	9.45	37.15		
LM-2	Siltstone	18.450	15.600	38.240	9.58	37.15		
LM-3	Siltstone	18.490	15.630	38.330	9.64	37.59		
LM-4	Sandstone	18.410	15.630	38.280	9.53	37.34		
LM-5	Siltstone	18.540	15.640	38.480	9.70	38.39		
LM-6	Siltstone	18.490	15.650	38.430	9.64	38.08		
MLP	Basement	19.850	15.720	39.360	11.42	42.83		

verify that the lead isotope compositions of the sulphides, other than galena, did not changed significantly since the time of ore formation we analysed the U, Th, and Pb concentrations in four sulphide samples. The analyses indicate that the values of both μ ($^{238}U/^{204}Pb$) and ω ($^{232}Th/^{204}Pb$) values are close to zero in three of the samples and somewhat higher (μ = 1.0 and ω = 3.8) in one (AR6–364.9, Table 3). These findings indicate that the calculated difference between the corrected values (believed to represent the time of ore formation of 145 Ma, see below) and the measured, present-day values in these sulphides is very small. The uniformity of the ore sulphide data is also reflected by the narrow ranges in the values of μ, mostly between 9.7 and 9.8, and ω, between 36 and 37, which were calculated using the model developed by Stacey and Kramers (1975) (Table 3). The model ages essentially define ranges of 50–90 Ma (Stacey and Kramers, 1975) and 90–130 Ma (Cumming and Richards, 1975).

The lead isotope compositions of the rocks span a significant interval; e.g., the measured $^{206}Pb/^{204}Pb$ ratios range from 18.58 to 20.08. The sedimentary rocks exhibit relatively uniform isotopic compositions that are similar to those of the ore sulphides, whereas the volcanic rocks exhibit more radiogenic compositions. The single mica schist sample from the basement has the most radiogenic composition of all the rocks (Table 3).

5.3. Sr isotopes

Rb–Sr isotopic data are listed in Table 4 and plotted in Fig. 6. The chlorite and rock samples are characterized in part by relatively high Rb/Sr ratios, which means that a few of the calculated initial $^{87}Sr/^{86}Sr$ ratios occasionally deviate significantly from the measured ratios. Analogous with the Pb system, εSr(i) values were calculated based on an age of 145 Ma. The εSr(i) values range from 24 to 265 in the sedimentary rocks and between 61 and 275 in the volcanic rocks from the Lemaire Fm. A few of the data from the latter appear to indicate some type of Rb-Sr disturbance because the calculated initial Sr isotope values are impossibly low in two of the volcanic rocks (Table 4). Chlorites from the hydrothermal alteration assemblages yielded εSr(i) values between 47 and 203. The εSr(i) value of the single mica schist sample from the basement is 121 (Table 4).

6. Discussion

6.1. Origin of sulphur and metals in the Arroyo Rojo deposit

The sulphide mineral assemblages in the orebody and the lack of barite and haematite suggest that the sulphur was present primarily as H_2S. The sulphides from the Arroyo Rojo deposit yielded $\delta^{34}S$ values ranging from very negative to slightly positive $\delta^{34}S$ values (−27.6 to 2.6‰), but most of the values range from −17 to 1.0‰. The total isotopic range is not significantly different from that of marine sediments reported by Ohmoto and Goldhaber (1997). The variation in $\delta^{34}S_{CDT}$ values in the Arroyo Rojo deposit is consistent with biogenic reduction of Late Jurassic seawater sulphate (~18‰) although the mineralizing fluids were relatively deficient in SO_4^{-2}, as suggested by the lack of sulphates in the deposit.

Although the distribution of sulphur isotope data at Arroyo Rojo is reasonably well explained by the effect of a low-temperature bacterial

Table 4
Sr and Rb concentrations, Sr isotopic compositions, and epsilon parameter for alteration chlorites and volcanic and sedimentary rocks from the Lemaire Formation. The decay constant used in the age calculation is: $\lambda^{87}Sr = 1.42 \times 10^{-11}$ year^{-1}. (xtal tuff (a): crystal-rich rhyolitic tuffites; xtal tuff (b): crystal-rich dacitic tuffites; prox: proximal; sm: semimassive, m: massive). No data with negative eps(i) are shown.

Sample	Type	Rb (ppm)	Sr (ppm)	$^{87}Sr/^{86}Sr$	$\pm 2\sigma$	$(^{87}Sr/^{86}Sr)i$	εSr_i
LM07-1	Sandstone	139	38	0.725593	12	0,7230	265
LM07-2	Siltstone	33	133	0.706060	8	0,7060	24
LM07-3	Siltstone	73	47	0.715164	18	0,7141	138
LM07-4	Sandstone	102	80	0.716391	10	0,7155	158
LM07-5	Siltstone	49	73	0.713419	10	0,7129	122
LM07-6	Siltstone	109	79	0.716216	8	0,7152	155
LMO	Rhyolite	131	62	0.723142	17	0,7216	246
BC6-4	Rhyolite	143	195	0.711210	3	0,7107	90
BS1-4	Rhyolite	252	41	0.728033	27	0,7237	275
BS1-6	xtal. Tuff (a)	190	102	0.719747	12	0,7184	200
PC-4	xtal. Tuff (b)	218	133	0.711063	15	0,7099	79
MLP	Basement	24	136	0.713013	8	0,7129	121
AR3-3C2	Chlorite (mass)	121	21	0.743123	31	0,7187	203
AR7-134C2	Chlorite (sm)	2	10	0.709338	14	0,7092	69
AR7-133C2	Chl (prox)	13	18	0.709909	13	0,7094	72
AR6-139C2	Chl (prox)	125	36	0.716224	11	0,7137	134
AR2-105C1	Chl (prox)	136	25	0.714181	20	0,7103	84
AR2-57C4	Chl (distal)	2	18	0.711445	20	0,7114	100
AR2-57C1	Chl (distal)	2	18	0.711333	26	0,7113	98
AR6-202C3	Chl (reg)	34	75	0.707995	5	0,7077	47
AR6-262.5C3	Chl (reg)	68	150	0.708192	17	0,7079	50

sulphate reduction (BSR), some of the heavier isotopic values indicates the entrainment of sulphur from other sources. In this study, the heavier $\delta^{34}S$ values (Fig. 5 and Table 2) are between ~0 and +3‰. In VMS deposits and their modern counterparts, the two sources of sulphur, apart from BSR, are: (1) seawater sulphate with variably positive $\delta^{34}S$ (Claypool et al., 1980; Paytan and Gray, 2012) that is present in sulphate minerals or is reduced by thermochemical sulphate reduction (TSR), and (2) deep-seated sulphur (leached from igneous footwall rocks and/or direct contributions from magmatic fluids) with $\delta^{34}S \approx -5$ to +5‰ (Ohmoto and Goldhaber, 1997). Brueckner et al. (2015) determined the relative contributions of these two sulphur sources using a mass balance model and concluded that the sulphur originated primarily from mixtures of TSR of seawater sulphate combined with deep subseafloor sulphur (sulphur leached from igneous wall rock and/or derived from magmatic fluids). In addition, they attributed stratigraphic variations in $\delta^{34}S$ to variations in the ratio of TSR to igneous sulphur, what may explain the observed difference in S isotope values between the lower ore lens (drill holes AR4 and AR6; Fig. 2C) and stratigraphically higher levels in the Arroyo Rojo deposit.

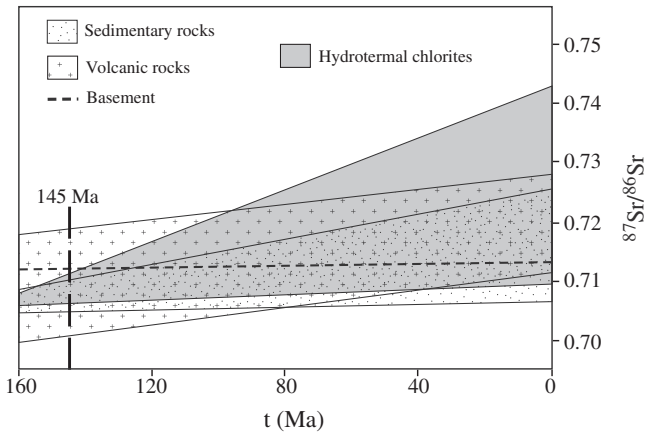

Fig. 6. Sr isotopic composition of hydrothermal chlorite compared with those of the possible Sr reservoirs at the time of ore formation (see text for details).

Metamorphism is occasionally capable of modifying the primary S isotope pattern in a deposit. However, despite the textures indicating metamorphism (Figs. 3G and H and 4D) are present at the Arroyo Rojo deposit, there is no correlation between the metamorphic textures and $\delta^{34}S$ values of the sulphides. This is suggesting that metamorphic re-equilibration of $\delta^{34}S$ was not a significant process for the sulphides in the Arroyo Rojo deposit, and hence S isotope compositions were controlled by surface-driven processes (Barrie et al., 2010).

It was previously argued that the effect of in-situ decay of Th and U in sulphides is insignificant. It therefore follows that the lead isotopic compositions are relatively uniform in the sulphides and chlorites in the ores and the proximal and distal alteration zones, whereas the composition of the chlorites in the zone of regional alteration is slightly more radiogenic. This pattern suggests that the lead in both the sulphides and ore-associated chlorites originated from the same source(s). This isotopic uniformity of the ore lead is consistent with that reported in VMS deposits in Australia (Gulson et al., 1984) and in the Iberian Pyrite Belt (Pomiès et al., 1998) and contrasts with the diversity of signatures observed in Kuroko-type deposits (Sato et al., 1981; Sasaki et al., 1982) and in modern submarine hydrothermal deposits (Fouquet and Marcoux, 1995). This uniformity implies that the lead in the ore-forming fluids originated from essentially crustal sources, in contrast to the presence of a significant mantle lead component in Kuroko-type deposits (Sato et al., 1981; Sasaki et al., 1982). Predominantly crustal control of the ore lead compositions is further indicated by Fig. 7, in which the data plot between curves representing the upper crust and the orogene.

A critical discussion of the sources of the ore lead requires that the rock data are corrected for the time of ore formation. The preferred age of ca. 145 Ma for the tuffites of the Lemaire Formation sets an approximative upper age limit of the ore formation. Furthermore, a plausible ore-forming model for a deposit of the Arroyo Rojo character implies a close temporal relationship between the Lemaire magmatism and the ore formation. Following this and noting that the oldest part of the overlying Yahgán Formation is approximately 144 Ma, i.e., nearly coeval with the declining stages of the Lemaire magmatism, the age of the ore formation is apparently constrained to ca 145 Ma.

Unfortunately, back-calculating the lead isotope data is limited by the fact that U, Th and Pb concentrations are available only from four of the volcanic rocks. The large variation in U/Pb and Th/Pb ratios (Table 3) suggests the possibility that certain rocks may have gained or lost elements due to fluid migration associated with ore-forming processes. Nevertheless, two assumptions were made to at least provide a qualitative estimate of the size of the correction needed to obtain initial lead isotope compositions of potential source rocks. First, the μ and ω values of the single volcanic rock lacking concentration data were arbitrarily set to 10 and 45, respectively. These values are typical of upper crustal rocks and are within the broad interval that characterizes the analysed rocks (Table 3). Second, noting that the sedimentary and volcanic rocks have similar lead isotope compositions and that the sedimentary rocks are thought to be partially composed of material from the local volcanic rocks, it was assumed that the μ and ω values assigned to the volcanic sequence can also be applied to the sedimentary rocks. Based on these assumptions, the approximate differences between the measured data and calculated initial lead isotopic compositions (at 145 Ma) for the rocks lacking concentration data (cf. Fig. 7) are 0.23 units ($^{206}Pb/^{204}Pb$), 0.01 units ($^{207}Pb/^{204}Pb$) and 0.33 units ($^{208}Pb/^{204}Pb$). These calculated differences are not highly dependent on the choice of μ and ω values from the perspective of evaluating sources of the ore lead. However, to account for the uncertainty in the analysis, the sizes of the symbols indicating the samples in Fig. 7 are made larger for rocks lacking concentration data. The initial lead isotope compositions of the rocks, back-calculated to the inferred time of ore formation (145 Ma), are shown in Fig. 7.

The uniformity of the isotopic compositions suggests that the lead was derived from a single source or that the ore-forming fluids

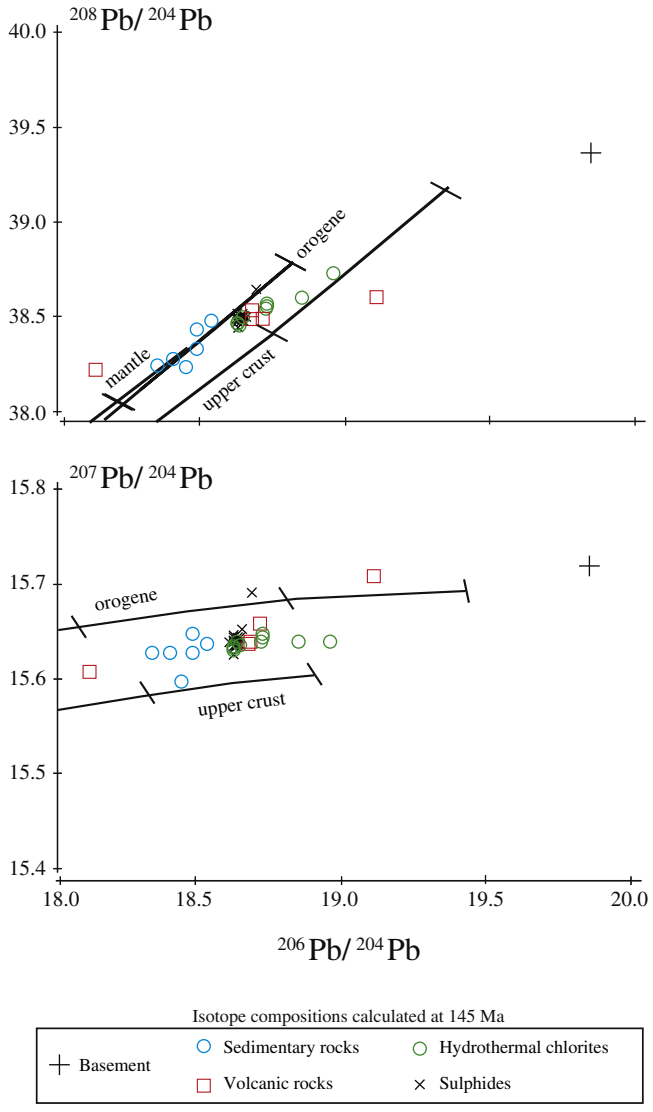

Fig. 7. Lead isotope data of the Arroyo Rojo deposit reported in $^{207}Pb/^{204}Pb$ and $^{208}Pb/^{204}Pb$ versus $^{206}Pb/^{204}Pb$ spaces. Lead isotope evolution curves were generated by the Plumbotectonic model (Zartman and Haines, 1988). Tick marks along each curve indicate progressively older time in 0.4 Ga increments.

contained lead from different sources and was homogenized prior to ore deposition due to mixing at great depths. However, neither of the host rock sequences in the Arroyo Rojo deposit had homogeneous Pb isotope compositions at 145 Ma. In fact, the only type of country rocks that is compatible with the Pb isotope values are the volcanic rocks. The sedimentary rocks, in contrast, appear to be characterized by less radiogenic values than the ore compositions.

The Sr isotopic data from the chlorites and sulphides also overlap, suggesting fluids of the same source. The initial (145 Ma) Sr isotope compositions of the chlorites strictly related to the massive and semimassive settings (values between ca. 0.708 and 0.709; Table 4) are in good agreement with the data from the siltstones. However, the possibility that strontium (and perhaps, other metals) was leached from both the clastic and volcanic host rocks also remains a likely explanation.

6.2. Origin and characteristics of the ore-forming fluids at Arroyo Rojo

The calculated $\delta^{18}O$ values of water in isotopic equilibrium with chlorite in the Arroyo Rojo deposit at the temperatures listed in Table 2 show a trend of heavier $\delta^{18}O$ values and lighter δD values with increasing distance from the ore bodies ($\delta^{18}O$ from +3.9 to 15.1‰ and δD from −15.1 to −51.2‰). Certain mechanisms such as evaporation, water/rock interactions, and boiling can promote ^{18}O enrichment but not the observed δD shift in the fluid. Given the constraint imposed by δD_{H2O} values of −50‰ or lower, a magmatic and/or metamorphic contribution is required. Therefore, our preferred explanation is that the $\delta^{18}O$ and δD covariation (Fig. 8) in the Arroyo Rojo samples is consistent with a binary mixing model involving an isotopically heavy fluid (Jurassic seawater) and an isotopically light fluid (magmatic water). Nevertheless, the seawater end-member must have evolved from one of 0‰ $\delta^{18}O$ to one of > + 6‰ $\delta^{18}O$ in response to isotope exchange with siliciclastic portions (generally material high in ^{18}O) of the underlying Lemaire Formation and the metamorphosed basement of the Lapataia Formation. This model is similar to models proposed for other VMS deposits such as the Blue Hill (Munha et al., 1986) and Kidd Creek deposits (Huston and Taylor, 1999).

Under the low-grade metamorphic conditions (greenschist facies) indicated by the mineral assemblages and phyllosilicate crystallinity, the δD and $\delta^{18}O$ values of the chlorites need not have been substantially affected. In fact, the marked variation in δD and $\delta^{18}O$ values in the Arroyo Rojo deposit suggests that extensive isotopic homogenization during metamorphism was unlikely.

The presence of halite as a daughter mineral in the primary fluid inclusions points to circulation of hot saline brines. The absence of evaporites in the study area rules out the possibility that the high-salinity fluids were derived from leaching of evaporite deposits by circulating seawater. Although other processes (e.g., shale membrane filtration, diagenetic hydration or maturation of Cl-rich illite to white mica) have been invoked to explain high-salinity fluids in other VMS deposits, the high $\delta^{18}O_{fluid}$ values at Arroyo Rojo are best explained by isotopic exchange with ^{18}O-enriched siliciclastic sediments.

6.3. A model for the Arroyo Rojo deposit

Two major models of volcanogenic massive sulphide formation at or near the sea floor have been proposed: (1) the Kuroko model (Ohmoto and Skinner, 1983), which involves mound building by chimney collapse and zone refining of the growing mound and (2) the brine-pool model (Solomon and Zaw, 1997), which involves hot and saline

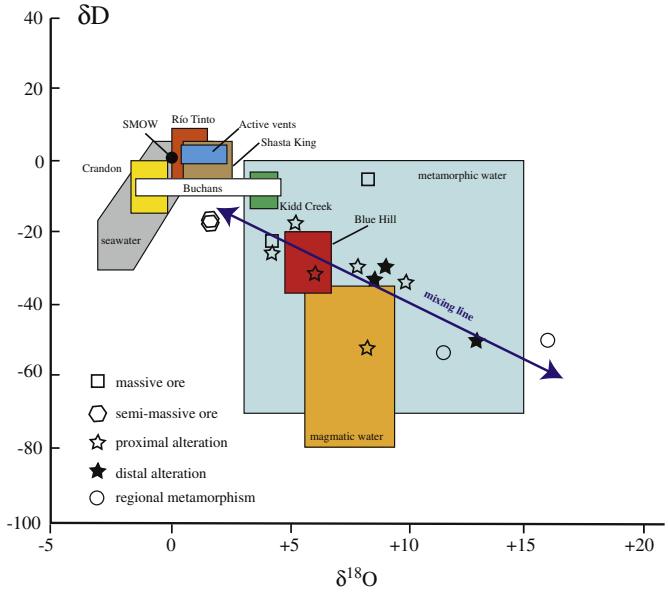

Fig. 8. $\delta^{18}O_{chlorite}$ vs. $\delta D_{chlorite}$ values (‰, in respect to V-SMOW) for Arroyo Rojo hydrothermal chlorites. Diagram also shows the fields of selected VMS ore-forming fluids (Huston, 1999), the fields of seawater, metamorphic water and metasediments (Shepperd, 1986) and magmatic water (Taylor, 1992).

hydrothermal fluids becoming negatively buoyant after mixing with seawater and subsequently being trapped in basins on the sea floor. Similar to the brine pool model, the accumulation of hydrothermal fluids at the bottom of the ocean with the formation of stratified layers as proposed by Goodfellow and Peter (1996) might also be invoked.

The Arroyo Rojo deposit differs from the "classic" Kuroko deposits in five aspects: (1) the lack of hydrothermal edifices and sulphates, (2) its stratiform morphology and stratabound hydrothermal alteration, (3) its abundance of framboidal and fine-grained pyrite, (4) reduced mineral assemblages (pyrite-pyrrhotite) and the (5) presence of saline fluids. These features meet the criteria proposed by Solomon et al. (2004) as typical for brine pool-type deposits, and this led Biel et al. (2010) to suggest that the Arroyo Rojo mineralisation formed in a brine pool. Yet, the presence of disseminated and semimassive sulphides developed around the massive orebodies hosted by volcaniclastic rocks, mainly composed of porous and reactive tuffaceous units, seem to indicate that subseafloor replacement processes generated a portion of the deposit. This process is consistent with Piercey's (2015) discussion of the importance of replacement processes in VMS deposits.

Our isotopic data from Arroyo Rojo suggest mixed sources of S, metals and hydrothermal fluids as a result of fluids of mixed magmatic and seawater origin interacting with underlying volcanic-sedimentary sequence. Two different sources for sulphur are plausible: reduced sulphate from seawater as a result of either bacteriogenic or thermochemical processes, or a combination of both, and magmatic sulphur (sulphur leached from igneous wall rock/derived from magmatic fluids). In addition, the uniform Pb isotopic compositions imply that isotopic homogenization of ore-forming fluids occurred at depth and prior to ore precipitation.

That is, hydrothermal fluids derived from seawater underwent a large water-rock interaction and mixed with upwelling magmatic fluids in order to acquire such homogeneous isotopic signature. A possible depositional setting for the Arroyo Rojo deposit would be a restricted and anoxic basin associated with carbonaceous turbidites along the flank of a rhyolitic flow-dome complex. The high permeabilities related to discrete networks of fractures in the rhyolitic breccia were favourable for the development of a stringer zone. Away from the stringer zone, lateral infiltration of hydrothermal fluids and replacement of host volcanic facies resulted in the formation of a halo of semimassive to disseminated ore. This part of the ore zone occurs as a stratabound replacement of porous and reactive tuffaceous units, mainly glassy and breccia tuffs. The hydrothermal fluids reaching an environment at the top of the stringer zone were expelled into the water column, which promoted more extensive sulphide precipitation by further dilution with seawater. Moderate ore fluid temperatures, below 300 °C, were responsible for the elevated (Zn + Pb)/Cu ratio of the deposit and the absence of zone refining.

The outlined model is coherent with the geodynamic context of the study area, that links to the initial breaking-up of Gondwana (Hanson and Wilson, 1991). The submarine volcanism of the Lemaire Formation is thought to represent widespread Jurassic extension and development of a narrow and deep-marine volcano-tectonic rift parallel to the Andean side of South America. The presence of a thick sedimentary sequence in a zone with crustal thinning, widespread extensional/strike-slip faulting, and a high geothermal gradient connected with widespread magmatic activity were all critical factors in the development of dynamic long-lived hydrothermal systems.

7. Conclusions

The Arroyo Rojo deposit is related to a submarine volcano-sedimentary complex that formed in a volcanic rift, specifically, the embryonic stage of a back-arc marginal basin during regional extension related to the onset of the Gondwana break-up during the Jurassic (ca. 145 Ma).

Stable isotope data (H, O) suggest that ore-forming fluids were dominated by seawater that underwent significant interaction with the underlying volcanic and sedimentary rocks. Such processes took place at depth and led to various degrees of isotopic (Sr, Pb) homogenization of ore fluids. S isotope data are largely consistent with bacteriogenic reduction of seawater sulphate, but some more positive values call for a certain contribution of sulphur resulting from inorganically reduction of seawater sulphate and magmatic sources. The hydrothermal fluids were channelized along faults promoting the formation of the stringer zone made up of quartz and sulphides and semi-massive and disseminated sulphides in favourable lithologies, mainly breccia and glassy tuffs. Further up in the stratigraphy, more massive and semimassive ore bodies developed near or on top of the seafloor.

Due to this proposed hydrothermal system, the Arroyo Rojo deposit exhibits two styles of mineralization: (1) a stringer zone and a halo of semi-massive to disseminated ore, which corresponding to sub-seafloor replacement, and (2) syn-sedimentary mineralization consisting of massive sulphides. In short, we conclude that the Arroyo Rojo deposit may represent an intermediate type between a brine-pool- and sub-seafloor replacement type of massive deposits.

Acknowledgements

This work was supported by the Spanish project CGL2007-61095 (Ministry of Science and Technology/Ministry of Education and Science and FEDER) and by the Regional Government of Aragón and the European Regional Development Fund (Grupos Consolidados) E-45 project. The work by C. Biel at the Swedish Natural History Museum (LIG) was funded by the Programa Europa CAI-CONAI. C. Biel is thankful for the Ministry of Education and Science pre-doctoral research fellowship. The authors also extend special thanks to Antonio Camprubí, and an anonymous reviewer, for their constructive, critical and helpful comments, which improved the manuscript greatly. This paper has also benefited from comments by Prof. Francisco Velasco (Universidad del País Vasco).

References

Acevedo, R.D., Fanlo, I., Subías, I., Paniagua, A., Buffone, D.E., 2005. Polymetallic VMS Deposits of the Andes Fueguinos (Southernmost Argentina): Preliminary Report. In: Mao, J., Bierlein, F.P. (Eds.), Mineral Deposit ResearchMeeting the Global Challenge vols. 1 and 2. Springer-Verlag, Berlin, Beijin, pp. 599–602.

Ametrano, S., Etcheverry, R., Echeveste, H., Godeas, M., Zubia, M., 2000. VMS District of Tierra del Fuego, Argentina. In: Sherlock, R., Logan, M.A.V. (Eds.), VMS Deposits of Latin America. Geological Association of Canada, pp. 593–612.

Barrie, C.D., Boyle, A.P., Cook, N.J., Prior, D.J., 2010. Pyrite deformation textures in the massive sulfide ore deposits of the Norwegian Caledonides. Tectonophysics 483, 269–286. http://dx.doi.org/10.1016/j.tecto.2009.10.024.

Biel, C., 2011. El depósito de sulfuros masivos polimetálicos de Arroyo Rojo, Tierra del Fuego (Argentina). Mineralogía, Geoquímica Y Metalogenia. Universidad de Zaragoza (Ph D.). (130 pp.).

Biel, C., Subías, I., Fanlo, I., Acevedo, R.D., 2007. Mineralogical Characterization of the Lemaire and Yahgán Formations, Tierra del Fuego, Argentina. In: Demant, A., Hervé, F., Menichetti, M., Tassone, A. (Eds.), GeoSur. Pontificia Universidad Católica de Chile, Santiago de Chile, p. 23.

Biel, C., Subías, I., Fanlo, I., Mateo, E., Acevedo, R.D., 2010. The Arroyo Rojo volcanic-hosted massive sulphide deposit (Tierra del Fuego, southernmost Argentina): geology, mineralogy, petrography and mineral chemistry. Rev. Mex. Cienc. Geol. 27, 84–96 (EID: 2-s2.0-77955951117).

Biel, C., Subías, I., Acevedo, R.D., Yusta, I., Velasco, F., 2012. Mineralogical, IR-spectral and geochemical monitoring of hydrothermal alteration in a deformed and metamorphosed Jurassic VMS deposit at Arroyo Rojo, Tierra del Fuego, Argentina. J. S. Am. Earth Sci. 35, 62–73. http://dx.doi.org/10.1016/j.jsames.2011.11.005.

Borrello, A.V., 1972. Cordillera Fueguina. In: Leanza, A.F.E. (Ed.), Geología Regional Argentina. Academia Nacional de Ciencias de Córdoba, Córdoba, pp. 741–754.

Broili, C., Klohn, M., Hodder, R.W., 2000. Exploration, Geology and Mineral Deposits in the Fin del Mundo Project, Tierra del Fuego, Argentina. In: Sherlock, R., Logan, M.A.V. (Eds.), VMS Deposits of Latin America. GAC Mineral Deposits Division, pp. 567–591.

Brueckner, S.M., Piercey, S.J., Layne, G.D., Piercey, G., Sylvester, P.J., 2015. Variations of sulphur isotope signatures in sulphides from the metamorphosed Ming Cu(−Au) volcanogenic massive sulphide deposit, Newfoundland Appalachians, Canada. Mineral. Deposita 50, 619–640. http://dx.doi.org/10.1007/s00126-014-0567-7.

Calderón, M., Fildani, A., Hervé, F., Fanning, C.M., Weislogel, A., Cordani, U., 2007. Late Jurassic bimodal magmatism in the northern sea-floor remnant of the Rocas Verdes basin, southern Patagonian Andes. J. Geol. Soc. Lond. 134, 1011–1022. http://dx.doi.org/10.1144/0016-76492006-102.

Caminos, R., 1980. Cordillera Fueguina. Geología Regional Argentina. Academia Nacional de Ciencias, Córdoba, pp. 1463–1501.
Caminos, R., Haller, M., Lapido, J., Lizuain, O., Page, A., Ramos, V.A., 1981. Reconocimiento geológico de los Andes Fueguinos. Territorio Nacional de Tierra del Fuego. Actas VIII Congr. Geol. Argent. 3, 759–786.
Canfield, D.E., Raiswell, R., Westrich, J.T., Reaves, C.M., Berner, R.A., 1986. The use of chromium reduction in the analysis of reduced inorganic sulfur in sediments and shales. Chem. Geol. 54, 149–155. http://dx.doi.org/10.1016/0009-2541(86)90078-1.
Cathelineau, M., 1988. Cation site occupancy in chlorites and illites as a function of temperature. Clay Miner. 23, 471–485. http://dx.doi.org/10.1180/claymin.1988.023.4.13.
Claypool, G.E., Holser, W.T., Kaplan, I.R., Sakai, H., Zak, I., 1980. The age curves of sulfur and oxygen isotopes in marine sulfate and their mutual interpretation. Chem. Geol. 28, 199–260. http://dx.doi.org/10.1016/0009-2541(80)90047-9.
Cumming, G.L., Richards, J.R., 1975. Ore lead isotope ratios in a continuously changing earth. Earth Planet. Sci. Lett. 28, 155–171. http://dx.doi.org/10.1016/0012-821X(75)90223-X.
Dalziel, I.W.D., Brown, R.L., 1989. Tectonic denudation of the Darwin metamorphic Core complex in the Andes of Tierra-del-Fuego, Southernmost Chile - implications for Cordilleran Orogenesis. Geology 17, 699–703. http://dx.doi.org/10.1130/0091-7613(1989)017%3C0699:TDOTDM%3E2.3.CO;2.
Eldridge, C.S., Barton, P.B., Ohmoto, H., 1983. Mineral textures and their bearing on formation of the Kuroko orebodies. Econ. Geol. Monogr. 5, 241–281.
Fallick, A.E., McConville, P., Boyce, A.J., Burguess, R., Kelley, S.P., 1992. Laser microprobe stable isotope measurements on geological materials: some experimental considerations (with special reference to $\delta^{34}S$ in sulphides). Chem. Geol. 101, 53–61.
Fildani, A., Hessler, A.M., 2005. Stratigraphic record across a retroarc basin inversion. Rocas Verdes – Magallanes Basin, Patagonian Andes: Geol. Soc. Am. Bull. 117, 1596–1614.
Fouquet, Y., Marcoux, E., 1995. Lead isotope systematics in Pacific hydrothermal sulfide deposits. J. Geophys. Res. 100, 6025–6040. http://dx.doi.org/10.1029/94JB02646.
Goodfellow, W.D., Peter, J.A., 1996. Sulphur isotope composition of the Brunswick No. 12 massive sulphide deposit, Bathurst Mining Camp: implications for ambient environment, sulphur source and ore genesis. Can. J. Earth Sci. 33, 231–251. http://dx.doi.org/10.1139/e96-020.
Graham, C.M., Atkinson, J., Harmon, R.S., 1987. Hydrogen Isotope Fractionation in the System Chlorite-Water. NERC 6th Progress Report of Research 1981–1984. NERC Publication Series D Vol. 25, p. 139.
Gulson, B.L., Korsch, M.J., Cameron, M., Vaasjoki, M., Mizon, K.J., Porritt, P.M., Carr, G.R., Kamper, C., Dean, J.A., Calvez, J.Y., 1984. Lead isotope ratio measurements using the Isomass 54E in fully automatic mode. Int. J. Mass Spectrom. Ion Process. 59, 125–142. http://dx.doi.org/10.1016/0168-1176(84)85090-9.
Hall, G.E.M., Pelchat, J.C., Loop, J., 1988. Separation and recovery of various sulphur species in sedimentary rocks for stable sulphur isotope determination. Chem. Geol. 67, 35–47. http://dx.doi.org/10.1016/0009-2541(88)90004-6.
Hanson, R.E., Wilson, T.J., 1991. Submarine Rhyolitic Volcanism in a Jurassic Proto-Marginal Basin; Southern Andes, Chile and Argentina. In: Harmon, R.S., Rapela, C.W. (Eds.), Andean Magmatism and its Tectonic Setting. Geological Society of America, Boulder, Colorado, pp. 13–27 http://dx.doi.org/10.1130/SPE265-p13.
Hervè, F., Nelson, E., Kawashita, K., Suarez, M., 1981. New isotopic ages and the timing of orogenic events in the Cordillera Darwin, southernmost Chilean Andes. Earth Planet. Sci. Lett. 55, 257–265. http://dx.doi.org/10.1016/0012-821X(81)90105-9.
Hervé, F., Pankhurst, R.J., Fanning, C.M., Calderón, M., Yaxley, G.M., 2007. The South Patagonian batholith: 150 my of granite magmatism on a plate margin. Lithos 97, 373–394.
Huston, D.L., 1999. Stable isotopes and their significance for understanding the genesis of volcanic-hosted massive sulfide deposits: a review. Rev. Econ. Geol. 8, 157–179.
Huston, D.L., Taylor, B.E., 1999. Genetic significance of oxygen and hydrogen isotope variations at the Kidd Creek volcanic-hosted massive sulphide deposit, Ontario, Canada. Econ. Geol. Monogr. 10, 335–350.
Kajiwara, Y., Krouse, H.R., 1971. Sulfur isotope partitioning in metallic sulfide systems. Can. J. Earth Sci. 8, 1397–1408. http://dx.doi.org/10.1139/e71-129.
Keith, M., Haase, K.M., Schwarz-Schampera, U., Klemd, R., Petersen, S., Bach, W., 2014. Effects of temperature, sulfur, and oxygen fugacity on the composition of sphalerite from submarine hydrothermal vents. Geology 42, 699–702. http://dx.doi.org/10.1130/G35655.1.
Kranck, E.H., 1932. Geological investigations in the cordillera of Tierra del Fuego. Acta Geogr. 4, 1–231.
Krogh, T.E., 1973. A low contamination method for hydrothermal decomposition of zircon and extraction of U and Pb for isotopic age determinations. Geochim. Cosmochim. Acta 37, 289–297. http://dx.doi.org/10.1016/0016-7037(73)90213-5.
Large, R.R., 1992. Australian volcanic-hosted massive sulfide deposits: features, styles, and genetic models. Econ. Geol. 97, 471–510.
Mukasa, S.B., Dalziel, I.W.D., 1996. Southernmost Andes and South Georgia Island, North Scotia Ridge: zircon U-Pb and muscovite $^{40}Ar/^{39}Ar$ age constraints on tectonic evolution of southwestern Gondwanaland. J. S. Am. Earth Sci. 9, 349–365. http://dx.doi.org/10.1016/S0895-9811(96)00019-3.
Munha, J., Barriga, J.A.S., Kerrich, R., 1986. High $^{18}0$ ore-forming fluids in volcanic-hosted base metal massive sulfide deposits: geologic, $^{18}O/^{16}O$, and D/H evidence from the Iberian Pyrite Belt; Crandon, Wisconsin; and Blue Hill, Maine. Econ. Geol. 81, 530–552.
Ohmoto, H., Goldhaber, M., 1997. Sulfur and Carbon Isotopes. In: Barnes, H.D. (Ed.), Geochemistry of Hydrothermal Ore Deposits, third ed., pp. 517–611.
Ohmoto, H., Skinner, B.J. (Eds.), 1983. The Kuroko and Related Volcanogenic Massive Sulfide Deposits. Economic Geology Monograph vol. 5 (604 pp.).
Olivero, E.B., Malumián, N., 2008. Mesozoic-Cenozoic stratigraphy of the Fuegian Andes, Argentina. Geol. Acta 6, 5–18.
Olivero, E.B., Martinioni, D.R., 2001. A review of the geology of the Argentinian Fuegian Andes. J. S. Am. Earth Sci. 14, 175–188.
Pankhurst, R.J., Leat, P.T., Srouga, P., Rapela, C.W., Márquez, M., Storey, B.C., Riley, T., 1998. The Chon Aike province of Patagonia and related rocks in West Antarctica: a silicic large igneous province. J. Volcanol. Geotherm. Res. 81 (1–2), 113–136. http://dx.doi.org/10.1016/S0377-0273(97)00070-X.
Paytan, A., Gray, E.T., 2012. Sulfur Isotope Stratigraphy. In: Gradstein, F.M., Ogg, J.G., Schmitz, M., Ogg, G. (Eds.), The Geologic Timescale 212. Elsevier, Amsterdam, pp. 167–180 http://dx.doi.org/10.1016/B978-0-444-59425-9.00009-3.
Piercey, S.J., 2015. A semipermeable interface model for the genesis of subseafloor replacement-type volcanogenic massive sulfide (VMS) deposits. Econ. Geol. 110 (7), 1655–1660. http://dx.doi.org/10.2113/econgeo.110.7.1655.
Pomiès, C., Cocherie, A., Guerrot, C., Marcoux, E., Lancelot, J., 1998. Assessment of the precision and accuracy of lead-isotope ratios measured by TIMS for geochemical applications: example of massive sulphide deposits (Rio Tinto, Spain). Chem. Geol. 144, 137–149. http://dx.doi.org/10.1016/S0009-2541(97)00127-7.
Sasaki, A., Sato, K., Cumming, G.L., 1982. Isotopic composition of ore lead from the japanese islands. Min. Geol. 32, 457–474.
Sato, K., Delevaux, M.H., Doe, B.R., 1981. Lead isotope measurements on ores, igneous and sedimentary rocks from the Kuroko mineralization area. Geochem. J. 15, 135–140. http://dx.doi.org/10.2343/geochemj.15.135.
Savin, S., Lee, M., 1988. Isotopic studies of phyllosilicates. Rev. Mineral. 19, 189–223.
Schermerhorn, L.J.G., 1978. Epigenetic magnesiam metasomatism or syngenetic chloritite metamorphism at Falun and Orijärvi. Inst. Min. Metall. Trans. Sect. B Appl. Earth Sci. 87, 162–167.
Sharp, Z.D., 1990. A laser-based microanalytical method for the in situ determination of oxygen isotope ratios of silicates and oxides. Geochim. Cosmochim. Acta 54, 1353–1357. http://dx.doi.org/10.1016/0016-7037(90)90160-M.
Shepperd, S.M.F., 1986. Characterization and Isotopic Variations in Natural Waters. In: Valley, J.W., Taylor, H.P., O'Neil, J.R. (Eds.), Stable Isotopes in High Temperature Geological ProcessesReviews in Mineralogy Vol. 16. Min. Soc. America, pp. 165–183.
Solomon, M., Zaw, K., 1997. Formation of the Hellyer volcanogenic massive sulfide deposit on the sea floor. Econ. Geol. 92, 686–695.
Solomon, M., Tornos, F., Large, R.R., Badham, J.N.P., Both, R.A., Zaw, K., 2004. Zn-Pb-Cu volcanic-hosted massive sulphide deposits: criteria for distinguishing brine pool-type from black smoker-type sulphide deposition. Ore Geol. Rev. 25, 259–283. http://dx.doi.org/10.1016/j.oregeorev.2004.01.003.
Stacey, J.S., Kramers, J.D., 1975. Approximation of terrestrial lead isotope evolution by a 2-stage model. Earth Planet. Sci. Lett. 26, 207–221. http://dx.doi.org/10.1016/0012-821X(75)90088-6.
Taylor, B.E., 1992. Degassing of H_2O from rhyolitic magma during eruption and shallow intrusion, and the isotopic composition of magmatic water in hydrothermal system. Geol. Surv. Jpn. Rep. 2789, 190–194.
Zartman, R.E., Haines, S.M., 1988. The plumbotectonic model for Pb isotopic systematics among major terrestrial reservoirs, a case for bidirectional transport. Geochim. Cosmochim. Acta 52, 1327–1339. http://dx.doi.org/10.1016/0016-7037(88)90204-9.